ELSEVIER

Chemical Engineering Journal 66 (1997) 11–20

CHEMICAL ENGINEERING JOURNAL

Modeling of liquid emulsion membranes facilitated by two carriers

Young Sun Mok [a], Won Kook Lee [b], Yong Kuk Lee [a,*]

[a] *Environment and Energy Research Team, Technical Research Laboratories, Pohang Iron and Steel Company Ltd., Pohang, PO Box 36, 1 Koedong-dong, Nam-ku, Pohang-shi, Kyungbuk 790-785, South Korea*

[b] *Department of Chemical Engineering, Korea Advanced Institute of Science and Technology, 373-1 Kusong-dong, Yusong-gu, Taejon 305-701, South Korea*

Received 26 July 1995; accepted 23 April 1996

Abstract

A mathematical model was proposed to describe the behavior of liquid emulsion membranes for the extraction of penicillin G in a continuous countercurrent mixing column. A polyamine-type surfactant acts not only as a carrier but also as a surface-stabilizing agent; thus the influence of surfactant on extraction should be considered in mathematical modeling when its effect is significant. The proposed model takes into account the influence of surfactant on mass transfer. The advancing front model was employed for deriving the overall mass transfer coefficient in the emulsion globule, and the axial dispersion model was applied to the external feed phase. The experimental data were compared with the proposed model, the calculations without considering the contribution of the surfactant to extraction, and the calculations without considering diffusion in the emulsion phase.

Keywords: Polyamine-type surfactant; Advancing front model; Axial dispersion model

1. Introduction

Liquid emulsion membranes provide a potentially powerful technique for effecting a diverse number of separation operations, while simultaneously allowing the extracted solute to be concentrated strongly in the receiving phase. In the industrial application of this technique, a continuous operation using a mixer–settler or a column is required. However, there have been only a few studies on the continuous process so far [1–6].

While some studies of potential applications of liquid emulsion membranes in biotechnology have appeared in recent literature, few models have been developed to describe and predict the extraction kinetics of organic acids [7–9]. Moreover, there have been no reports on the continuous extraction model of organic acids by liquid emulsion membranes.

When liquid emulsion membranes are applied to the organic acid extraction such as carboxylic acids and penicillin G, the use of a polyamine-type surfactant can give rise to an increase in extraction rate [10–12]. To confirm the role of surfactant as a carrier, Hano et al. [11] performed extraction experiments using emulsions prepared with various surfactant concentrations. The results show that the use of ECA 4360J as a surfactant considerably facilitates the extraction of penicillin G even without any other carriers. Therefore, a quantitative estimate of the role of the surfactant becomes necessary to describe accurately the behavior of liquid emulsion membranes. Nevertheless, none of the modeling studies in the literature include the influence of the surfactant on organic acid transport.

The objective of this work is to develop a model, which includes the influence of a surfactant on the extraction, for a continuous separation process by liquid emulsion membranes. Liquid emulsion membrane operations are well described by the advancing front model [13,14]. On the basis of this model, the overall mass transfer coefficient in the emulsion globule was derived by considering the contribution of the surfactant. With this overall mass transfer coefficient, the axial dispersion model was applied to the external feed phase. In this work, extraction experiments were performed in a countercurrent mixing column with penicillin G, and the concentration profiles along the column were measured in order to be compared with the model.

2. Theory

2.1. Transport mechanism of penicillin

Let us consider an emulsion globule containing the carrier dissolved in the membrane phase. The solute present in the

* Corresponding author.

PII S1385-8947(96)03147-8

external feed phase diffuses through the external aqueous film and undergoes the reaction with the carrier at the interface between the external feed phase and the membrane phase to form a complex. This reaction equilibrium can be expressed as follows [15]:

$$H^+(aq) + P^-(aq) + A(org) \Leftrightarrow AHP(org) \quad (1)$$

$$K_{eq,1} = \frac{C_{m1}}{C_H C_p C_{B1}} = 3.0\ m^6\ mol^{-2} \quad (2)$$

where C_{m1} is the concentration of the complex made of penicillin G and the carrier, C_p is the penicillin G anion concentration, C_H is the proton concentration and C_{B1} is the carrier concentration.

Similarly, the reaction equilibrium of penicillin G with the surfactant is equated as

$$H^+(aq) + P^-(aq) + S(org) \Leftrightarrow SHP(org) \quad (3)$$

$$K_{eq,1} = \frac{C_{m2}}{C_H C_p C_{B2}} = 1.01\ m^6\ mol^{-2} \quad (4)$$

where C_{m2} is the concentration of the complex made of penicillin G and the surfactant and C_{B2} is the surfactant concentration.

The two complexes formed at the external interface diffuse through the membrane phase to the interface between the membrane and the internal phases. At this interface, the acid anion is stripped from the complex by the stripping reagent and the carrier diffuses back to the feed side of the membranes.

A model of an emulsion globule is schematically depicted in Fig. 1, which describes the increase in diffusion length with the increase in degree of extraction. If no internal circulation occurs within the emulsion globule, the diffusion distance becomes increasingly longer because the complexes formed at the external interface diffuse into the emulsion globule up to the radius where there are internal droplets containing unreacted stripping reagent. A reaction front is assumed to exist within the emulsion globule which separates an unreacted reagent core from the internal droplets containing the reaction products, as shown in Fig. 1. This reaction front will gradually advance toward the center of the emulsion globule as the solute in the external feed phase is removed.

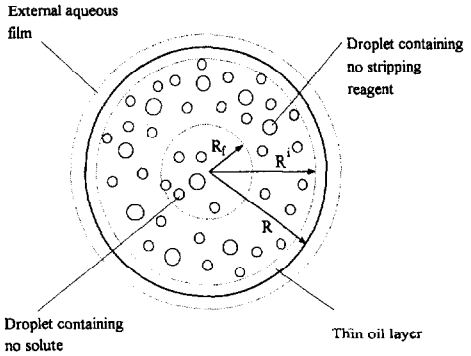

Fig. 1. Schematic diagram of an emulsion globule.

2.2. Overall mass transfer coefficient

Mass transfer will take place between the external feed phase and the advancing reaction front at any position in the column. Three mass transfer resistances may be considered in mathematical analysis of this system:

1. diffusion in the external aqueous film
2. diffusion in the thin oil layer
3. diffusion in the emulsion phase

As presented in Fig. 2, the concentration profile of each component in the emulsion globule is assumed to be linear.

The flux in the external aqueous film is related to the mass transfer coefficient in the external aqueous film as follows:

$$J_e = k(C_p - C_p^*) \quad (5)$$

where k is the mass transfer coefficient in the external feed phase and C_p^* is the penicillin G anion concentration at the interface between the external and membrane phases.

The carrier concentration can be assumed to be uniform in the emulsion globule and equal to its initial concentration since the solute–carrier complex is constantly removed by the stripping reagent. The pH can be assumed to be kept constant in the column when a buffer solution is used. From the equilibrium constant, C_p^* can be expressed as follows:

$$C_p^* = \frac{C_{m1}^*}{K_{eq,1} C_H C_{B1}} \quad (6)$$

If quasi-steady state is assumed, the flux of the solute–carrier complex in the thin oil layer is given as

$$J_1 = \frac{D_{m1}}{\delta}\frac{R_i}{R}(C_{m1}^* - C_{m1}') \text{ in the thin oil layer } (R_i < r < R) \quad (7)$$

where D_{m1} is the diffusivity of the solute–carrier complex, δ is the thickness of the thin oil layer and C'_{m1} is the complex concentration at R_i.

According to Fig. 2, J_1 is also equated as follows:

$$J_1 = \frac{D_{c1}}{R_i - R_f}\frac{R_f}{R_i} C_{m1}' \text{ in the emulsion phase } (R_f < r < R_i) \quad (8)$$

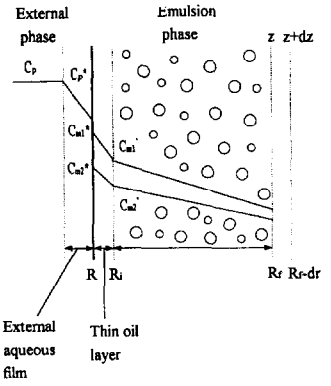

Fig. 2. Concentration profile of each component in the emulsion globule, assuming quasi-steady state.

where D_{e1} is the effective diffusivity of the solute–carrier complex in the emulsion phase and R_f is the radius of the advancing front.

When the series resistances are considered, the flux can be expressed as follows:

$$J_1 = K_1 C^*_{m1} \tag{9}$$

where

$$\frac{1}{K_1} = \frac{\delta}{D_{m1}}\frac{R}{R_i} + \frac{R_i - R_f}{D_{e1}}\frac{R_i}{R_f} \tag{10}$$

For the solute–surfactant complex, similar equations are obtained:

$$J_2 = K_2 C^*_{m2} \tag{11}$$

where

$$\frac{1}{K_2} = \frac{\delta}{D_{m2}}\frac{R}{R_i} + \frac{R_i - R_f}{D_{e2}}\frac{R_i}{R_f} \tag{12}$$

In Eqs. (11) and (12), the subscript 2 indicates the solute–surfactant complex.

From a mass balance, the flux J_e is equal to the sum of the two fluxes J_1 and J_2:

$$J_e = J_1 + J_2 \tag{13}$$

Substituting Eqs. (59) and (11) into Eq. (13) gives

$$k\left(C_p - \frac{C^*_{m1}}{K_{eq,1} C_H C_{B1}}\right) = K_1 C^*_{m1} + K_2 C^*_{m2} \tag{14}$$

From Eqs. (2) and (4), the expression for C_{m2} can be obtained with respect to C_{m1} as follows:

$$C_{m2} = \frac{K_{eq,2}}{K_{eq,1}}\frac{C_{B2}}{C_{B1}} C_{m1} \tag{15}$$

Eq. (14) can be rewritten by substitution of Eq. (15):

$$J_e = k\left(C_p - \frac{C^*_{m1}}{K_{eq,1} C_H C_{B1}}\right) = \left(K_1 + K_2 \frac{K_{eq,2} C_{B2}}{K_{eq,1} C_{B1}}\right) C^*_{m1} \tag{16}$$

Rewriting Eq. (16) in terms of the overall mass transfer coefficient:

$$J_e = K_o C^*_p \tag{17}$$

where

$$\frac{1}{K_o} = \frac{1}{k} + \frac{1}{K_{eq,1} C_H C_{B1}} \frac{1}{K_1 + K_2 (K_{eq,2}(C_{B2}/K_{eq,1})/C_{B1})} \tag{18}$$

It should be noted that the concentration of penicillin G anion in a reacted internal droplet is equal to the concentration of sodium ion. Thus, from the material balance, the radius of the reaction front is given by

$$\frac{R_f}{R_i} = \left\{1 - \frac{(1-h)(C_{e,0} - C_e)}{2h\phi C_{i,0}}\right\}^{1/3} \tag{19}$$

Here, C_e is the total concentration of the solute, i.e. undissociated penicillin G and penicillin G anion, and it can be written as follows:

$$C_e = C_p + C_{HP} = C_p(1 + 10^{pK_a - pH}) \tag{20}$$

2.3. Mathematical model

Fig. 3 shows a model of a continuous countercurrent column operation. The feed, an aqueous phase containing the solute, is supplied at the top of the column as the continuous phase. The dispersed phase, a water-in-oil (W/O) emulsion, is supplied at the bottom of the column and flows countercurrently with the feed phase in the column. The surfactant in the membrane phase satisfactorily stabilizes the W/O emulsion, and the W/O emulsion is finely dispersed in the feed phase, resulting in a large mass transfer area.

The concentration profile in the countercurrent column is influenced by mass transfer in the external aqueous film and diffusion in the emulsion globule. It is also influenced by the column type and the axial dispersion.

For devices in which the concentration of the dissolved solute changes continuously with axial distance, on the assumption that the axial mixing can be adequately described by an axial dispersion coefficient, the material balance over a differential height of the column for the external feed phase is

$$E_c \frac{d^2 C_p}{dz^2} + u_c \frac{dC_p}{dz} - ka(C_p - C^*_p) = 0 \tag{21}$$

where E_c is the axial dispersion coefficient of the external feed phase, u_c is the superficial velocity of the external feed

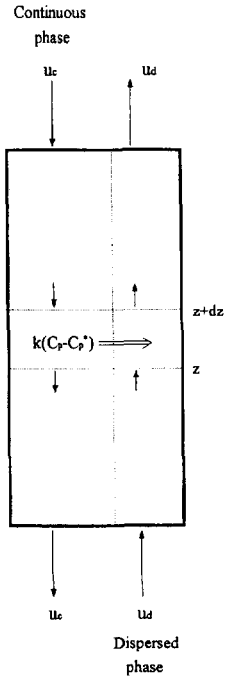

Fig. 3. Modeling of column.

phase, a is the superficial area of contact of the phases and z is the axial distance.

Eq. (21) can be rewritten with respect to the overall mass transfer coefficient as follows:

$$E_c\frac{d^2C_p}{dz^2}+u_c\frac{dC_p}{dz}-K_oaC_p=0 \tag{22}$$

From the holdup of the dispersed phase, Eq. (22) can be rewritten as follows:

$$E_c\frac{d^2C_p}{dz^2}+u_c\frac{dC_p}{dz}-\frac{3hK_o}{R}C_p=0 \tag{23}$$

The boundary conditions, obtained by material balance at each end of the column, are

$$z=0 \quad \frac{dC_p}{dz}=0 \tag{24}$$

$$z=L \quad -E_c\frac{dC_p}{dz}=u_c(C_p-C_{p,0}) \tag{25}$$

The equations can be cast in dimensionless form by defining

$$y=\frac{C_p}{C_{p,0}},\ N_{Pe}=\frac{u_cL}{E_c},\ Z=\frac{z}{L},\ N_c=\frac{3hLk}{Ru_c},\ \kappa_o=\frac{K_o}{k},\ \kappa_1=\frac{K_1}{k},$$

$$\kappa_2=\frac{K_2}{k},\ \sigma_1=K_{eq.1}C_HC_{B1},\ \sigma_2=K_{eq.2}C_HC_{B2} \tag{26}$$

The resulting equations are as follows:

$$\frac{1}{N_{Pe}}\frac{d^2y}{dZ^2}+\frac{dy}{dZ}-N_c\kappa_oy=0 \tag{27}$$

$$\kappa_o=1+\frac{1}{\sigma_1}\frac{1}{\kappa_1+\kappa_2\sigma_2/\sigma_1} \tag{28}$$

If the contribution of surfactant to mass transfer is negligible, the dimensionless overall mass transfer coefficient reduces to

$$\kappa_o=1+\frac{1}{\sigma_1}\frac{1}{\kappa_1} \tag{29}$$

Boundary conditions are

$$Z=0 \quad \frac{dy}{dZ}=0 \tag{30}$$

$$Z=1 \quad 1-y=\frac{1}{N_{Pe}}\frac{dy}{dZ} \tag{31}$$

Eq. (27) may be solved numerically by using the FORTRAN subroutine DBVPFD in the International Mathematical and Statistical Library (IMSL).

Two factors not accounted for in the modeling approach are the effects of breakage and emulsion swelling on extraction performance. If sufficient surfactant is included in the oil membrane phase, the breakage can be neglected. Swelling occurs primarily owing to the osmotic transport of water from the external feed phase to the encapsulated internal reagent droplets. In this system, a buffer solution prepared for keeping pH constant can also decrease the osmotic pressure difference between the external phase and the internal phase, i.e. the swelling caused by the osmotic pressure difference.

2.4. Parameter estimation

The mass transfer coefficient in the external feed phase was estimated from a correlation for mass transfer in an agitated vessel [16]. Although it was initially developed to correlate behavior in a batch system, the equation may be used for mass transfer to dispersed liquid drops in a continuous countercurrent column. Since the flow rates of the feed phase and the dispersed phase are small in this system, it can be successfully regarded as an agitated vessel.

$$\frac{k}{\sqrt{ND_{ex}}}=2.932\times10^{-7}h^{-0.508}\left(\frac{d_s}{D_T}\right)^{0.548}N_{Re}^{1.37} \tag{32}$$

where D_{ex} is the molecular diffusivity of the solute in the external aqueous film, d_s is the stirrer diameter, $N_{Re}=\rho_cd_s^2N/\mu_c$, ρ_c is the density of the external feed phase and μ_c is the viscosity of the external feed phase.

The thickness δ of the thin oil layer may be evaluated by the equation obtained by Lee and Chan [17].

The molecular diffusivity can be estimated by the Wilke–Chang [18] equation. The effective diffusivity in the heterogeneous emulsion phase may be calculated with the Maxwell equation which states that diffusion does not depend on the size of internal droplets but only on the volume fraction in the emulsion globule [19].

The axial dispersion coefficient was estimated by using the equation correlated for a mechanically agitated liquid extraction tower [20], and it is described by

$$\frac{(1-h)E_c}{u_cl_c}=-0.14+0.0268\frac{d_sN(1-h)}{u_c} \tag{33}$$

where d_s is the stirrer diameter and l_c is the compartment height.

2.5. Analytical solution

Eq. (27) can be solved analytically when the overall mass transfer coefficient is constant. If the diffusion in the emulsion phase is ignored, K_1 and K_2 reduce to

$$\frac{1}{K_1}=\frac{\delta}{D_{m1}}\frac{R}{R_i} \tag{34}$$

$$\frac{1}{K_2}=\frac{\delta}{D_{m2}}\frac{R}{R_i} \tag{35}$$

Since Eqs. (34) and (35) are constants, the overall mass transfer coefficient becomes a constant. Then, the concentration distribution of the solute in the column is given by [5]

$$y = \frac{2(1+q)\exp\{-(1/2)N_{Pe}(1-q)Z\} - 2(1-q)\exp\{-(1/2)N_{Pe}(1+q)Z\}}{(1+q)^2\exp\{-(1/2)N_{Pe}(1-q)\} - (1-q)^2\exp\{-(1/2)N_{Pe}(1+q)\}} \quad (36)$$

where

$$q = \{1 + (4N_c\kappa_o/N_{Pe})\}^{1/2} \quad (37)$$

3. Experimental details

3.1. Materials

The membrane phase was prepared by mixing kerosene (Junsei Chemical Co.) as the diluent, Amberlite LA2 (Sigma Chemical Co.) as the carrier, and ECA 4360J (Exxon Chemical Co.) as the surfactant. Sodium carbonate used as the stripping reagent was supplied from Junsei Chemical Company. Penicillin G ($pK_a = 2.75$) was obtained as its potassium salt from Sigma Chemical Company.

Citrate buffer solution, used as the external aqueous phase, was prepared to maintain constant pH in the external feed phase. It was composed of a mixture of citric acid and trisodium citrate. The total concentration of the buffer solution was 408 mol m^{-3}. In this system, emulsion swelling by osmotic pressure, which is the most serious problem in liquid emulsion membranes, can hardly occur during extraction due to the presence of the buffer solution.

3.2. Extraction in a continuous countercurrent column

A stable W/O emulsion was prepared by initially dissolving surfactant and carrier in kerosene and then adding Na_2CO_3 solution under high shear (200 rev s^{-1}) provided by a homogenizer (Tekmar, Germany). The emulsion thus prepared was fed from the bottom of the column at the desired flow rate. The feed phase was supplied at the top of the column at the desired flow rate. The emulsion drops supplied at the bottom rose to the top of the column and coalesced.

The continuous countercurrent mixing column was used for penicillin G extraction with liquid emulsion membranes, and details of its geometry are listed in Table 1. For measuring the concentration profile along the column, four sampling ports are fitted to the side of the column and one valve was fitted to the bottom of the column for taking the raffinate (total of five sampling ports). The column has nine stirrers and nine stators.

Table 1
Geometry of countercurrent mixing column

Column length	$L = 0.5$ m
Column diameter	$D_T = 0.062$ m
Height of each stage	$l_c = 0.045$ m
Stirrer diameter	$d_s = 0.028$ m
Number of stirrers	9
Number of sampling ports	5

Table 2
Typical experimental conditions

Feed concentration	20 mol m^{-3}
Stripping reagent concentration	200 mol m^{-3}
Carrier concentration	20 mol m^{-3}
Surfactant concentration	8 wt%
Feed phase pH	5
Membrane phase	Kerosene
Volume fraction of the internal phase in the emulsion	0.35
Flow rate u_c of feed phase	6.93×10^{-4} m s^{-1}
Flow rate u_d of dispersed phase	1.73×10^{-4} m s^{-1}
Stirrer speed	5.5 rev s^{-1}

At steady state, samples were taken from the sampling ports, filtered to remove the W/O emulsion drops, and the concentrations of the penicillin G were analyzed by high performance liquid chromatography (Waters) using 70 parts of phosphate buffer solution (100 mol m^{-3}) (a mixture of sodium dihydrogenphosphate dihydrate and disodium hydrogen phosphate dodecahydrate) at pH 7.8 to 30 parts of methanol as the mobile phase and a μ-Bondapak C_{18} column with a UV photometric detector (254 nm).

The holdup of the dispersed phase was determined by measuring the volume of the emulsion phase in the column after inlet and outlet cocks were simultaneously stopped. The W/O/W multiple emulsion was separated by density difference, and the volume of the separated W/O emulsion was measured.

The emulsion globule sizes were measured photographically, and the Sauter mean diameter was calculated. The mean internal droplet size was measured by a centrifugal particle size analyzer (SA-CP3, Shimadzu).

The reaction equilibrium constant of penicillin G with Amberlite LA2 or ECA 4360J was obtained by using the usual two-phase experiments. The organic solution was prepared by dissolving Amberlite LA2 or ECA 4360J (15–140 mol m^{-3}) in kerosene, and citrate buffer solutions (408 mol m^{-3}) were prepared at pH 4.8–6.0, and penicillin G potassium salt (5–250 mol m^{-3}) was dissolved in the buffer solutions. Equal volumes of the prepared organic and aqueous solutions were shaken in a flask for 4 h.

The molecular weight of ECA 4360J was determined to be 635 by cryoscopy, a technique for determining the molecular weight of a substance by dissolving it and measuring the freezing point of the solution [21].

Experiments involving changing several variables were carried out. When one variable was studied, all the other variables were kept constant at the values listed in Table 2.

4. Results and discussion

Fig. 4 shows the concentration profiles along the column length at the typical experimental conditions where the cal-

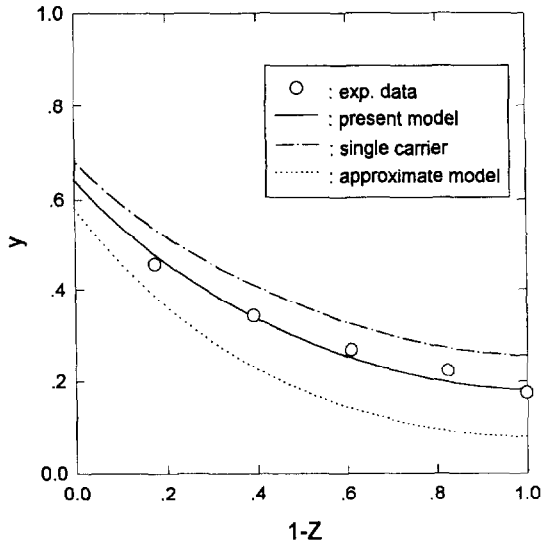

Fig. 4. Comparison of experimental with calculated results at typical conditions ($R=1.8\times10^{-4}$ m; $h=0.1740$; $k=1.963\times10^{-6}$ m s^{-1}; $D_{m1}=1.55\times10^{-10}$ m^2 s^{-1}; $D_{m2}=1.017\times10^{-10}$ m^2 s^{-1}; $D_{e1}=8.574\times10^{-11}$ m^2 s^{-1}; $D_{e2}=5.626\times10^{-11}$ m^2 s^{-1}; $R_\mu=1.38\times10^{-6}$ m; $N_{Pe}=2.586$).

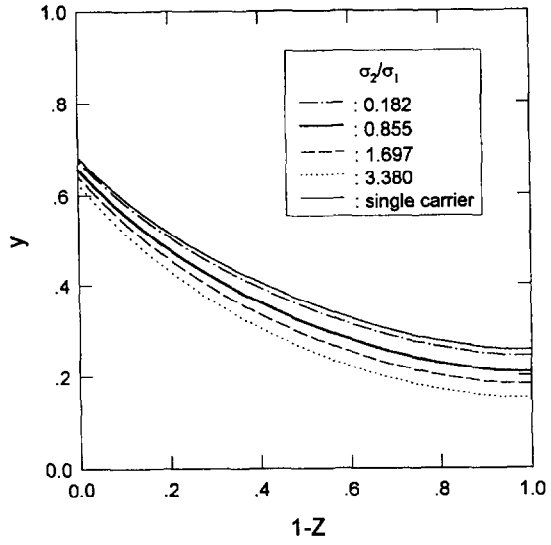

Fig. 5. Simulation results ($R=1.8\times10^{-4}$ m; $h=0.1740$; $k=1.963\times10^{-6}$ m s^{-1}; $D_{m1}=1.55\times10^{-10}$ m^2 s^{-1}; $D_{m2}=1.017\times10^{-10}$ m^2 s^{-1}; $D_{e1}=8.574\times10^{-11}$ m^2 s^{-1}; $D_{e2}=5.62\times10^{-11}$ m^2 s^{-1}; $R_\mu=1.38\times10^{-6}$ m; $N_{Pe}=2.586$).

culated results are also presented. The chain curve is the results calculated with Eq. (29), and the broken curve is the results calculated with Eqs. (34)–(36). As can be seen, the model (full curve) satisfactorily predicts the experimental data while the results without considering the influence of surfactant underestimate the experimental data and the results without considering the diffusion in emulsion phase overestimate the experimental data. These demonstrate that the contribution of surfactant to the transport rate and the diffusion in the emulsion phase cannot be neglected and should be taken into account in mathematical modeling.

4.1. Simulation results

The results in Fig. 5 show that an increase in σ_2/σ_1 gives rise to enhancement in mass transfer. The model calculations are performed by changing σ_2 with σ_1 unchanged. The concentration of surfactant in the membrane phase should also affect the interfacial penicillin G concentration. As the ratio σ_2/σ_1 decreases, the model approaches the calculation results considering only the transport by carrier (full curve), i.e. the influence of surfactant becomes less important. Therefore the contribution of surfactant to concentration profile can be neglected if the ratio σ_2/σ_1 is very small. Since the surfactant concentration is sufficiently high in order to maintain the emulsion stability, the necessary condition that the influence of surfactant on extraction is negligible is when the equilibrium constant $K_{eq,2}$ between the solute and the surfactant is small. In this system, however, $K_{eq,2}$ is not small compared with $K_{eq,1}$, and hence the model considering the influence surfactant is valid.

The influence of holdup of dispersed phase on the concentration distribution in the column is presented in Fig. 6 where the calculation results are also presented. When the stripping

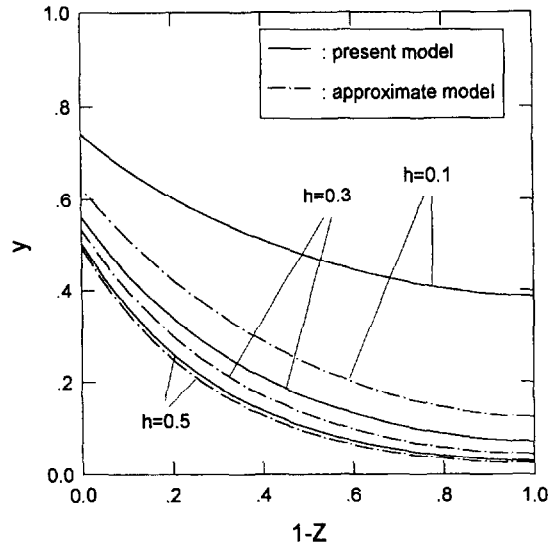

Fig. 6. Simulation results ($R=1.8\times10^{-4}$ m; $h=0.1740$; $k=1.963\times10^{-6}$ m s^{-1}; $D_{m1}=1.55\times10^{-10}$ m^2 s^{-1}; $D_{m2}=1.017\times10^{-10}$ m^2 s^{-1}; $D_{e1}=8.574\times10^{-11}$ m^2 s^{-1}; $D_{e2}=5.626\times10^{-11}$ m^2 s^{-1}; $R_\mu=1.38\times10^{-6}$ m; $N_{Pe}=2.586$).

reaction occurs only at the internal droplets close to the emulsion globule surface, the diffusion in the emulsion phase can be neglected. The large holdup makes it possible that the stripping reaction occurs at the internal droplets close to the emulsion globule surface. The same situation may take place when the concentration of the stripping reagent is high. The approximate model not considering the diffusion in the emulsion phase approaches the present model at large holdup of the dispersed phase. On the contrary, the difference between the present model and the approximate model is very large when the holdup of the dispersed phase is small. In other words, the approximate model is valid only for large holdup

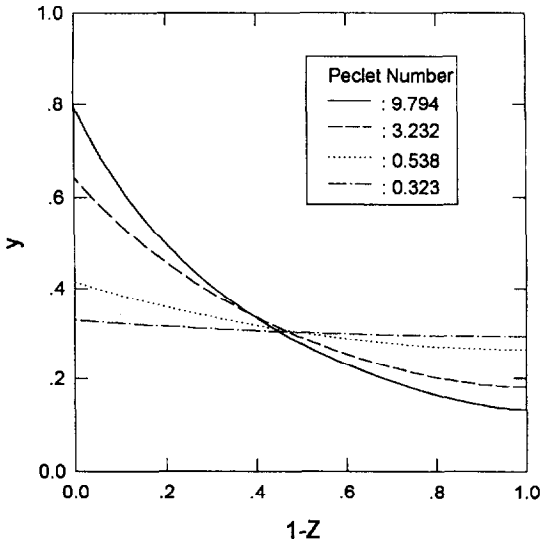

Fig. 7. Simulation results ($R=1.8\times10^{-4}$ m; $h=0.1740$; $k=1.963\times10^{-6}$ m s^{-1}; $D_{m1}=1.55\times10^{-10}$ m^2 s^{-1}; $D_{m2}=1.017\times10^{-10}$ m^2 s^{-1}; $D_{e1}=8.574\times10^{-11}$ $m^2\,s^{-1}$; $D_{e2}=5.626\times10^{-11}$ $m^2\,s^{-1}$, $R_\mu=1.38\times10^{-6}$ m, $N_{Pe}=2.586$).

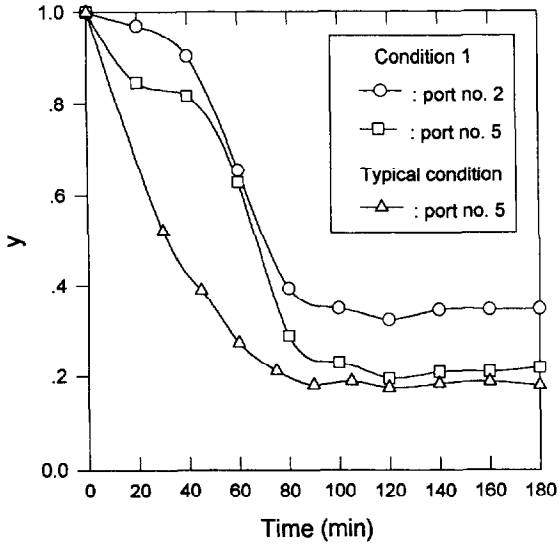

Fig. 8. Non-steady-state extraction behavior in the countercurrent mixing column.

because the diffusion in the emulsion phase becomes less important.

Fig. 7 shows the concentration profile along the column as a function of the Peclet number. At constant flow rate, the Peclet number decreases as the axial dispersion increases or the column length decreases. As can be seen in Fig. 7, the decrease in the Peclet number results in a decrease in the inlet concentration and an increase in the outlet concentration, and finally both concentrations become the same. To reduce the outlet concentration to within the acceptable limits, the Peclet number should be increased, i.e. the axial dispersion should be decreased or the column length should be increased. If the residual solute concentration at the bottom of the column is not within the acceptable limits, it should be discarded; several units of this type can be used in series to achieve a high degree of extraction.

4.2. Comparison of experimental data with computed results

To investigate the validity of the model, the experimental data are compared with the computed results. Fig. 8 shows the experimental results for the non-steady-state behavior of extraction. In condition 1, the flow rates of the external feed phase and the emulsion are 5.2×10^{-4} and 1.38×10^{-4} m s^{-1} respectively, and the volume fraction of the internal phase in the emulsion is 0.5. The other conditions are the same as in Table 2. As can be seen in the figure, steady states are attained in 90–120 min. Thus, samplings in all experiments are carried out after 120 min.

Fig. 9 depicts the influence of the stirrer speed on the concentration profile along the column. The experiments were carried out by changing the stirrer speed from 4.67 to 6.5 rev s^{-1}. The increase in the stirrer speed increases the surface

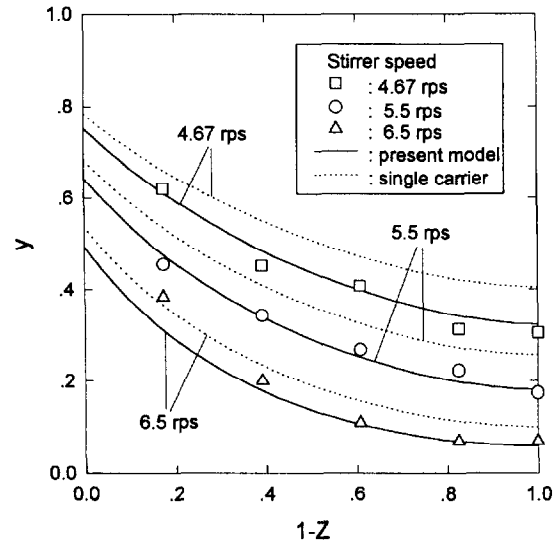

Fig. 9. Effect of stirrer speed on the concentration profile along the column ($D_{m1}=1.55\times10^{-10}$ m^2 s^{-1}; $D_{m2}=1.017\times10^{-10}$ m^2 s^{-1}; $D_{e1}=8.574\times10^{-11}$ $m^2\,s^{-1}$; $D_{e2}=5.626\times10^{-11}$ $m^2\,s^{-1}$; $R_\mu=1.38\times10^{-6}$ m). At 4.67 rev s^{-1}, $R=2.0\times10^{-4}$ m, $h=0.1359$, $k=1.639\times10^{-6}$ m s^{-1} and $N_{Pe}=3.058$; at 5.5 rev s^{-1}, $R=1.8\times10^{-4}$ m, $h=0.1740$, $k=1.963\times10^{-6}$ m s^{-1} and $N_{Pe}=2.586$; at 6.5 rev s^{-1}, $R=1.4\times10^{-4}$ m, $h=0.2174$, $k=2.396\times10^{-6}$ m s^{-1} and $N_{Pe}=2.180$.

area available for mass transfer, and decreases the mass transfer resistance in the external aqueous film. The holdup of the dispersed emulsion phase also increases with the stirrer speed. Therefore, the degree of extraction increases as the stirrer speed increases. The broken curves are the calculation results without considering the effect of the second carrier (surfactant). As can be seen, the model considering the contribution of the surfactant predicts more correctly the experimental data than do the calculations without the contribution of the surfactant.

The property of the organic solvent constituting a liquid membrane plays an important role in extraction rate. The

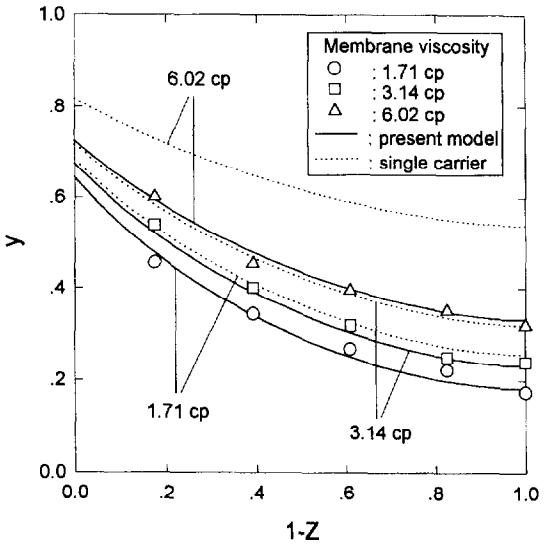

Fig. 10. Effect of membrane viscosity on the concentration profile along the column. At 1.71 cp, $R=1.8\times10^{-4}$ m, $h=0.1740$, $k=1.963\times10^{-6}$ m s^{-1}, $D_{m1}=1.55\times10^{-10}$ m^2 s^{-1}, $D_{m2}=1.017\times10^{-10}$ m^2 s^{-1}, $D_{e1}=8.574\times10^{-11}$ m^2 s^{-1}, $D_{e2}=5.626\times10^{-11}$ m^2 s^{-1}, $R_\mu=1.38\times10^{-6}$ m and $N_{Pe}=2.586$; at 3.14 cp, $R=2.0\times10^{-4}$ m, $h=0.1740$, $k=1.963\times10^{-6}$ m s^{-1}, $D_{m1}=1.24\times10^{-10}$ m^2 s^{-1}, $D_{m2}=0.81\times10^{-10}$ m^2 s^{-1}, $D_{e1}=6.83\times10^{-11}$ m^2 s^{-1}, $D_{e2}=4.48\times10^{-11}$ m^2 s^{-1}, $R_\mu=1.26\times10^{-6}$ m and $N_{Pe}=2.584$; at 6.02 cp, $R=2.5\times10^{-4}$ m, $h=0.1467$, $k=2.14\times10^{-6}$ m s^{-1}, $D_{m1}=0.694\times10^{-10}$ m^2 s^{-1}, $D_{m2}=0.455\times10^{-10}$ m^2 s^{-1}, $D_{e1}=3.84\times10^{-11}$ m^2 s^{-1}, $D_{e2}=2.52\times10^{-11}$ m^{2}s^{-1}, $R_\mu=1.185\times10^{-6}$ m and $N_{Pe}=2.582$.

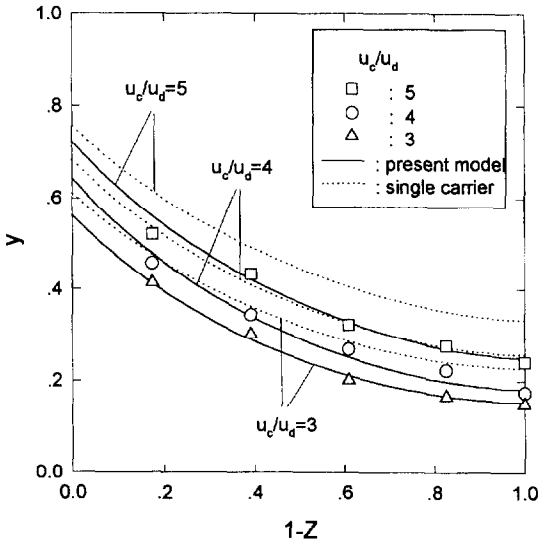

Fig. 11. Effect of external feed phase velocity on the concentration profile along the column ($R=1.8\times10^{-4}$ m; $D_{m1}=1.55\times10^{-10}$ m^2 s^{-1}; $D_{m2}=1.017\times10^{-10}$ m^2 s^{-1}; $D_{e1}=8.574\times10^{-11}$ m^2 s^{-1}; $D_{e2}=5.626\times10^{-11}$ m^2 s^{-1}, $R_\mu=1.38\times10^{-6}$ m). For $u_c/u_d=6$, $h=0.1609$, $k=2.043\times10^{-6}$ m s^{-1} and $N_{Pe}=3.940$; for $u_c/u_d=5$, $h=0.1565$, $k=2.071\times10^{-6}$ m s^{-1} and $N_{Pe}=3.255$; for $u_c/u_d=4$, $h=0.1740$, $k=1.963\times10^{-6}$ m s^{-1} and $N_{Pe}=2.586$; for $u_c/u_d=3$, $h=0.1685$, $k=1.995\times10^{-6}$ m s^{-1} and $N_{Pe}=1.921$.

concentration profiles along the column are measured by changing the viscosity of the membrane phase using liquid paraffin. The other conditions are the same as in Table 2. The variation in the concentration profile with the dimensionless axial distance is presented in Fig. 10. As the liquid paraffin content increases, the extraction becomes slow owing to a decrease in diffusivity and surface area. These results are quite consistent with the well-known fact that the less viscous membrane enhances the extraction of the solute across the membrane. It is observed that the holdup of the dispersed phase is low in the case of 40 wt% liquid paraffin as a result of the abrupt increase in the emulsion viscosity, which also makes the extraction rate low. The results calculated with the present model are in good agreement with the experimental data.

Fig. 11 shows the influence of the flow rate of the external feed phase at a constant flow rate of the dispersed phase on the concentration profile along the column. The degree of extraction decreases with the increase in the flow rate of the external feed phase because the contact time of the external phase with the dispersed phase is decreased. It is observed that the holdup of the dispersed phase does not vary greatly as a result of the flow rate of the external feed phase, which means that the holdup is more significantly affected by the stirrer speed or the physical properties of the emulsion itself. The calculation results are also shown in Fig. 11. The present model gives a much better approximation over the entire range.

As the volume fraction of the internal phase in the emulsion increases, the emulsion viscosity increases, and thus the surface area available for mass transfer decreases. In addition, the holdup of the dispersed phase decreases with increasing volume fraction of the internal phase. Thus the degree of extraction decreases with the volume fraction of the internal

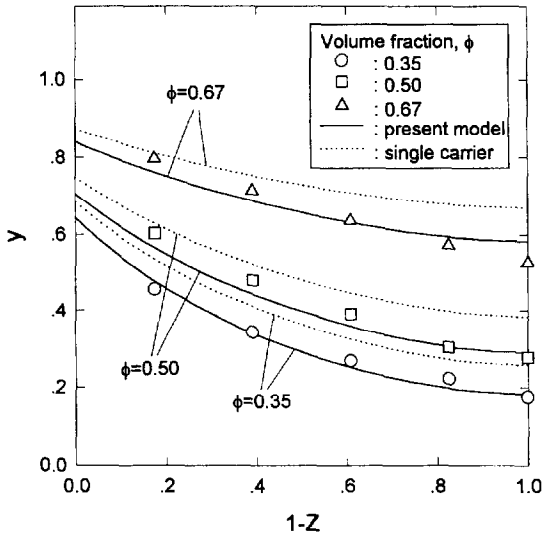

Fig. 12. Effect of internal phase volume fraction on the concentration profile along the column ($D_{m1}=1.55\times10^{-10}$ m^2 s^{-1}, $D_{m2}=1.017\times10^{-10}$ m^2 s^{-1}). For $\phi=0.35$, $R=1.8\times10^{-4}$ m, $h=0.1740$, $k=1.963\times10^{-6}$ m s^{-1}, $D_{e1}=8.574\times10^{-11}$ m^2 s^{-1}, $D_{e2}=5.626\times10^{-11}$ m^2 s^{-1}, $R_\mu=1.38\times10^{-6}$ m and $N_{Pe}=2.586$; for $\phi=0.5$, $R=1.9\times10^{-4}$ m, $h=0.1228$, $k=2.343\times10^{-6}$ m s^{-1}, $D_{e1}=6.2\times10^{-11}$ m^2 s^{-1}, $D_{e2}=4.068\times10^{-11}$ m^2 s^{-1}, $R_\mu=1.58\times10^{-6}$ m and $N_{Pe}=2.58$; for $\phi=0.67$, $R=2.8\times10^{-4}$ m, $h=0.0783$, $k=2.946\times10^{-6}$ m s^{-1}, $D_{e1}=3.831\times10^{-11}$ m^2 s^{-1}, $D_{e2}=2.514\times10^{-11}$ m^2 s^{-1}, $R_\mu=2.06\times10^{-6}$ m and $N_{Pe}=2.576$.

phase, which is shown in Fig. 12. The decrease in the holdup with the volume fraction of the internal phase results from large emulsion globule size and poor dispersion caused by high emulsion viscosity. The model calculations predict the experimental data well.

5. Conclusions

A mathematical model for liquid emulsion membranes was proposed to describe the continuous extraction of organic acid in a countercurrent mixing column. The proposed model gave a significant improvement in the accuracy over the previous models. The model can be successfully applied not only to a system where the surfactant used acts as a carrier but also to a system where two carriers are used to enhance the extraction performance of liquid emulsion membranes. The advancing front model was employed for the emulsion globule, and the axial dispersion model was applied to the external feed phase. The experimental data were satisfactorily predicted by the proposed model. On the contrary, neither the calculations without considering the contribution of the surfactant to extraction nor the calculations without considering the diffusion in the emulsion phase were in good agreement with the experimental data, indicating that the transport by the surfactant and the diffusion in the emulsion phase are important factors to be considered. The simulation results show that the calculations without considering the effect of the surfactant approach the present model as the equilibrium constant between the solute and the surfactant decreases, and the calculations without considering the diffusion in the emulsion phase approach the present model as the holdup of the dispersed phase increases.

Appendix A. Nomenclature

A	Carrier
a	Superficial area of contact of the phases (m^{-1})
aq	Aqueous phase
C_{B1}	Carrier concentration in the membrane phase (mol m^{-3})
C_{B2}	Surfactant concentration in the membrane phase (mol m^{-3})
C_e	Total solute concentration in the external phase (mol m^{-3})
C_H	Proton concentration (mol m^{-3})
$C_{i,o}$	Initial concentration of stripping reagent (mol m^{-3})
C_{m1}	Concentration of solute–carrier complex (mol m^{-3})
C_{m2}	Concentration of solute–surfactant complex (mol m^{-3})
C_p	Penicillin G anion concentration in the external phase (mol m^{-3})
$C_{p,0}$	Initial feed concentration (mol m^{-3})
d_s	Diameter of the stirrer (m)
D_T	Diameter of the column (m)
D_{e1}	Effective diffusivity of solute–carrier complex ($m^2\ s^{-1}$)
D_{e2}	Effective diffusivity of solute–surfactant complex ($m^2\ s^{-1}$)
D_{ex}	Molecular diffusivity of the solute in the external aqueous film ($m^2\ s^{-1}$)
D_{m1}	Diffusivity of solute–carrier complex ($m^2\ s^{-1}$)
D_{m2}	Diffusivity of solute–surfactant complex ($m^2\ s^{-1}$)
E_c	Axial dispersion coefficient of the external feed phase ($m^2\ s^{-1}$)
H^+	Hydrogen ion
h	Holdup of the dispersed phase (–)
J_1	Flux of solute–carrier complex (mol $m^{-2}\ s^{-1}$)
J_2	Flux of solute–surfactant complex (mol $m^{-2}\ s^{-1}$)
J_c	Flux of penicillin G anion in the external phase (mol $m^{-2}\ s^{-1}$)
k	Mass transfer coefficient in the external phase ($m\ s^{-1}$)
K_a	Acidic dissociation constant (mol m^{-3})
$K_{eq,1}$	Equilibrium constant of penicillin G with carrier ($m^6\ mol^{-2}$)
$K_{eq,2}$	Equilibrium constant of penicillin G with surfactant ($m^6\ mol^{-2}$)
K_1	Mass transfer coefficient of solute–carrier complex obtained by considering the series resistances in the thin oil film and the emulsion ($m\ s^{-1}$)
K_2	Mass transfer coefficient of solute–surfactant complex obtained by considering the series resistances in the thin oil film and the emulsion ($m\ s^{-1}$)
K_o	Overall mass transfer coefficient ($m\ s^{-1}$)
l_c	Compartment height (m)
L	Column length
N	Stirrer speed ($rev\ s^{-1}$)
N_{Pe}	Lu_c/E_c, Peclet number
org	Organic phase
P^-	Penicillin anion
R	Radius of emulsion globule (m)
R_f	Radius of advancing front (m)
R_i	Radius of inner core of emulsion globule (m)
S	Surfactant
u_c	Superficial velocity of the external feed phase ($m\ s^{-1}$)
u_d	Superficial velocity of the dispersed phase ($m\ s^{-1}$)
y	$C_p/C_{p,0}$, dimensionless concentration of penicillin G anion
z	Axial distance (m)
Z	z/L, dimensionless axial distance

A.1. Greek letters

δ	Thickness of the thin oil film (m)
μ_c	Viscosity of the external aqueous phase (kg $m^{-1}\ s^{-1}$)

ρ_c Density of the external aqueous phase (kg m^{-3})
ϕ Volume fraction of the internal phase in the emulsion phase

A.2. Superscript

* Interface between the external phase and the membrane phase

References

[1] R. Marr, M. Prötsch, J. Draxler and A. Kriechbaumet, *Ger. Chem. Eng., 6* (1983) 365.
[2] T.A. Hatton and D.S. Wardius, *AIChE J., 30* (1984) 934.
[3] M. Matsumoto, K. Ema, K. Kondo and F. Nakashio, *J. Chem. Eng. Jpn., 23* (1990) 402.
[4] C.C. Wang and A.L. Bunge, *Membr. Sci., 53* (1990) 105.
[5] T. Kataoka, T. Nishiki, M. Yamauchi and Y. Zhong, *J. Chem. Eng. Jpn., 20* (1987) 410.
[6] R. Rautenbach and O. Machhammer, *J. Membr. Sci., 36* (1988) 425.
[7] J.B. Chaudhuri and D.L. Pyle, *Chem. Eng. Sci., 47* (1992) 41.
[8] M. Teramoto, T. Yamashiro, A. Inoue, A. Yamamoto, H. Matsuyama and Y. Miyake, *J. Membr. Sci., 58* (1991) 11.
[9] H. Reisinger and R. Marr, *J. Membr. Sci., 80* (1993) 85.
[10] H. Reisinger and R. Marr, *Chem. Eng. Technol., 15* (1992) 363.
[11] T. Hano, T. Ohtake, M. Matsumoto, S. Ogawa and F. Hori, *J. Chem. Eng. Jpn., 23* (1990) 772.
[12] T. Hano, T. Ohtake, M. Matsumoto and S. Ogawa, *J. Membr. Sci., 84* (1993) 271.
[13] W.S. Ho, T.A. Hatton, E.N. Lightfoot and N.N. Li, *AIChE J., 28* (1982) 662.
[14] K.S. Kim, S.J. Choi and S.K. Ihm, *Ind. Eng. Chem. Fundam., 22* (1983) 167.
[15] M. Reschke and K. Schügerl, *Chem. Eng. J., 28* (1984) B1.
[16] A.H.P. Skelland and J.M. Lee, *AIChE J., 27* (1981) 99.
[17] C.J. Lee and C.C. Chan, *Ind. Eng. Chem. Res., 29* (1990) 101.
[18] C.R. Wilke and P. Chang, *AIChE J., 1* (1955) 264.
[19] E.L. Cussler, *Mass Transfer in Fluid Systems*, Cambridge University Press, Cambridge, UK, 1992, Chapter 7.
[20] R.E. Bibaud and R.E. Treybal, *AIChE J., 12* (1966) 472.
[21] J.A. Dean, Cryoscopic constants, in *Lange's Handbook of Chemistry*, 13th edn., McGraw–Hill, New York, 1985, pp. 10–80.